www.advenergymat.de

# On the Beneficial Impact of $Li_2CO_3$ as Electrolyte Additive in NCM523 $\parallel$ Graphite Lithium Ion Cells Under High-Voltage Conditions

Sven Klein, Patrick Harte, Jonas Henschel, Peer Bärmann, Kristina Borzutzki, Thomas Beuse, Stefan van Wickeren, Bastian Heidrich, Johannes Kasnatscheew, Sascha Nowak, Martin Winter,\* and Tobias Placke\*

Lithium ion battery cells operating at high-voltage typically suffer from severe capacity fading, known as 'rollover' failure. Here, the beneficial impact of  $\text{Li}_2\text{CO}_3$  as an electrolyte additive for state-of-the-art carbonate-based electrolytes, which significantly improves the cycling performance of NCM523  $\parallel$  graphite full-cells operated at 4.5 V is elucidated. LIB cells using the electrolyte stored at 20 °C (with or without  $\text{Li}_2\text{CO}_3$  additive) suffer from severe capacity decay due to parasitic transition metal (TM) dissolution/deposition and subsequent Li metal dendrite growth on graphite. In contrast, NCM523  $\parallel$  graphite cells using the  $\text{Li}_2\text{CO}_3$ -containing electrolyte stored at 40 °C display significantly improved capacity retention. The underlying mechanism is successfully elucidated: The rollover failure is inhibited, as  $\text{Li}_2\text{CO}_3$  reacts with  $\text{LiPF}_6$  at 40 °C to in situ form lithium difluorophosphate, and its decomposition products in turn act as 'scavenging' agents for TMs (Ni and Co), thus preventing TM deposition and Li metal formation on graphite.

#### 1. Introduction

Lithium ion batteries (LIBs) are the state-of-the-art battery technology dominating the market for various high-energy applications such as electro-mobility.<sup>[1]</sup> However, to achieve a satisfactory market acceptance of electric vehicles, it is mandatory

S. Klein, P. Harte, Dr. J. Henschel, P. Bärmann, T. Beuse, S. van Wickeren, B. Heidrich, Dr. S. Nowak, Prof. M. Winter, Dr. T. Placke University of Münster MEET Battery Research Center Institute of Physical Chemistry Corrensstraße 46, Münster 48149, Germany E-mail: tobias.placke@uni-muenster.de Dr. K. Borzutzki, Dr. J. Kasnatscheew, Prof. M. Winter

Dr. K. Borzutzki, Dr. J. Kasnatscheew, Prof. M. Winter Helmholtz-Institute Münster IEK-12 Forschungszentrum Jülich GmbH

Corrensstraße 46, Münster 48149, Germany

E-mail: m.winter@fz-juelich.de

The ORCID identification number(s) for the author(s) of this article can be found under https://doi.org/10.1002/aenm.202003756.

© 2021 The Authors. Advanced Energy Materials published by Wiley-VCH GmbH. This is an open access article under the terms of the Creative Commons Attribution License, which permits use, distribution and reproduction in any medium, provided the original work is properly cited.

DOI: 10.1002/aenm.202003756

to achieve sufficient driving ranges of at least 500 km at an affordable cost.<sup>[1a,2]</sup> The development of advanced LIB cell chemistries, that is, through novel negative (anode) and positive (cathode) active materials, is widely regarded as the most important strategy to accomplish further energy density improvements and cost savings.<sup>[1a,3]</sup>

Major improvements in terms of energy density can be achieved by advancements of the cathode, which is considered as 'bottleneck' in terms of specific capacity. [1a] State-of-the-art cathode materials are LiMO<sub>2</sub>-type layered oxides ( $M=\mathrm{Ni}$ , Co, Mn, Al, etc.), particularly including Li[Ni<sub>x</sub>Co<sub>y</sub>Mn<sub>z</sub>]O<sub>2</sub> (x+y+z=1; NCMxyz), because of their high theoretical capacities of up to  $\approx$ 280 mAh g<sup>-1</sup>. [2a,3a,4] However, only a limited amount of lithium can be

extracted from the NCM material at low cut-off potentials (e.g., ≤4.3 V vs. Li|Li<sup>+</sup>). A highly pursued approach to increase the specific capacity of low Ni (≤60%) NCM cathodes is to increase the cell voltage, resulting in a higher delithiation degree.<sup>[3a,5]</sup> However, this approach is known to result in severe capacity fading caused by various aging processes, such as oxidative electrolyte decomposition and subsequent impedance rise at the cathode. [2a,3a,4b,6] Besides structural degradation and changes at the cathode electrolyte interphase (CEI),[6,7] a major degradation mechanism of highvoltage (HV) operated LIB cells is due to cross-talk phenomena,[8] that is, dissolution of transition metals (TMs) from the cathode (e.g., Co<sup>2+</sup>, Ni<sup>2+</sup>, Mn<sup>2+</sup>). The TMs can migrate via the electrolyte and deposit at the anode surface, leading to a significant impedance rise by the degradation of the solid electrolyte interphase (SEI).[8c,9] A HV-operation of NCM-based cathodes (cell voltage ≥4.4 V) typically results in fast and severe capacity fading, known as 'rollover' failure. [9c,10] Previously, we demonstrated that the deposition of TM cations (Co<sup>2+</sup>, Ni<sup>2+</sup>, Mn<sup>2+</sup>) at graphite-based anodes resulted in significant SEI growth and Li metal dendrite formation in NCM523 || graphite full-cells operated at 4.5.[11] These dendrites resulted in a rollover failure, caused by penetration of dendrites through the separator to the cathode, thus, leading to the generation of (micro-)short-circuits.<sup>[11]</sup>

A straightforward strategy to improve the performance of HV-LIB cells is the use of electrolyte additives, preventing or diminishing the direct contact of electrolyte and electrode www.advancedsciencenews.com www.advenergymat.de

ADVANCED ENERGY MATERIALS

materials via in situ formation of interphases (SEI, CEI).  $^{[5,12]}$  Among various electrolyte additives, lithium difluorophosphate (LiDFP) has been shown to be a promising candidate for performance improvements of NCM  $\parallel$  graphite cells, in particular at  $\geq$ 4.4  $V^{[13]}$  It is well known that preparation and storage conditions (e.g., temperature) of electrolyte formulations significantly impact the chemical electrolyte stability, thus, the electrochemical performance.

Here, we unravel the positive impact of  $\rm Li_2CO_3$  as an electrolyte additive in NCM523  $\parallel$  graphite full-cells at 4.5 V, which prevents the HV-induced rollover failure caused by deposited TMs at the anode. Graphite anodes from NCM523  $\parallel$  graphite full-cells were comprehensively analyzed after cycling with respect to the deposition of Co, Ni, and Mn and a subsequent Li metal dendrite formation in terms of lateral elemental distribution. We can elucidate the underlying mechanism of in situ formed electrolyte decomposition products with respect to the beneficial impact of 'scavenging' dissolved TM species in the electrolyte.

#### 2. Results and Discussion

#### 2.1. Rollover Failure of High-voltage NCM523 | Graphite Full-cells

The cycling performance of NCM523 || graphite cells operated at 4.3 or 4.5 V, both using the standard electrolyte

('STD@20 °C'; 1 M LiPF<sub>6</sub> in EC:EMC 3:7 by wt.; stored at 20 °C), is depicted in **Figure** 1a. The cells operated at 4.5 V show an early induced 'rollover' failure after  $\approx$ 50 cycles, caused by TM deposition (Ni, Mn, Co), significant SEI growth and Li metal dendrite formation, which subsequently results in the generation of (micro-)short-circuits, as discussed in a previous work.<sup>[11]</sup> In contrast, the LIB cells operated at 4.3 V do not show any rollover failure and a rather stable capacity over 100 cycles.

Wang et al. showed that the use of Li<sub>2</sub>CO<sub>3</sub> as electrolyte additive can effectively reduce the dissolution of Mn<sup>2+</sup> ions from the LiMn<sub>2</sub>O<sub>4</sub> cathode at an operation temperature of 55 °C thus resulted in significant performance improvement of LiMn<sub>2</sub>O<sub>4</sub> || Li metal cells (3.0-4.35 V vs. Li|Li+).[14] As demonstrated by Choi et al., [15] it is particularly challenging to dissolve Li<sub>2</sub>CO<sub>3</sub> in carbonate-based electrolytes, which is not surprising as Li<sub>2</sub>CO<sub>3</sub> is known as a hardly soluble key component of the inorganic part of the SEI layer at anodes (e.g., graphite).[16] To elucidate the beneficial impact of Li<sub>2</sub>CO<sub>3</sub> as additive, we performed a systematic study. First, 1 wt% of Li<sub>2</sub>CO<sub>3</sub> was added to 'STD@20 °C' and was stored at 20 °C for 3 days to achieve a high solubility. Afterwards, the electrolyte was filtered to completely remove the remaining Li<sub>2</sub>CO<sub>3</sub> (white solid). The modified electrolyte ('STD+Li<sub>2</sub>CO<sub>3</sub>@20 °C') was examined in NCM523 || graphite full-cells operated at 4.5 V. However, in contrast to the work of Wang et al., [14] the addition of Li2CO3 does not result in an improved capacity retention. In fact, both electrolytes with

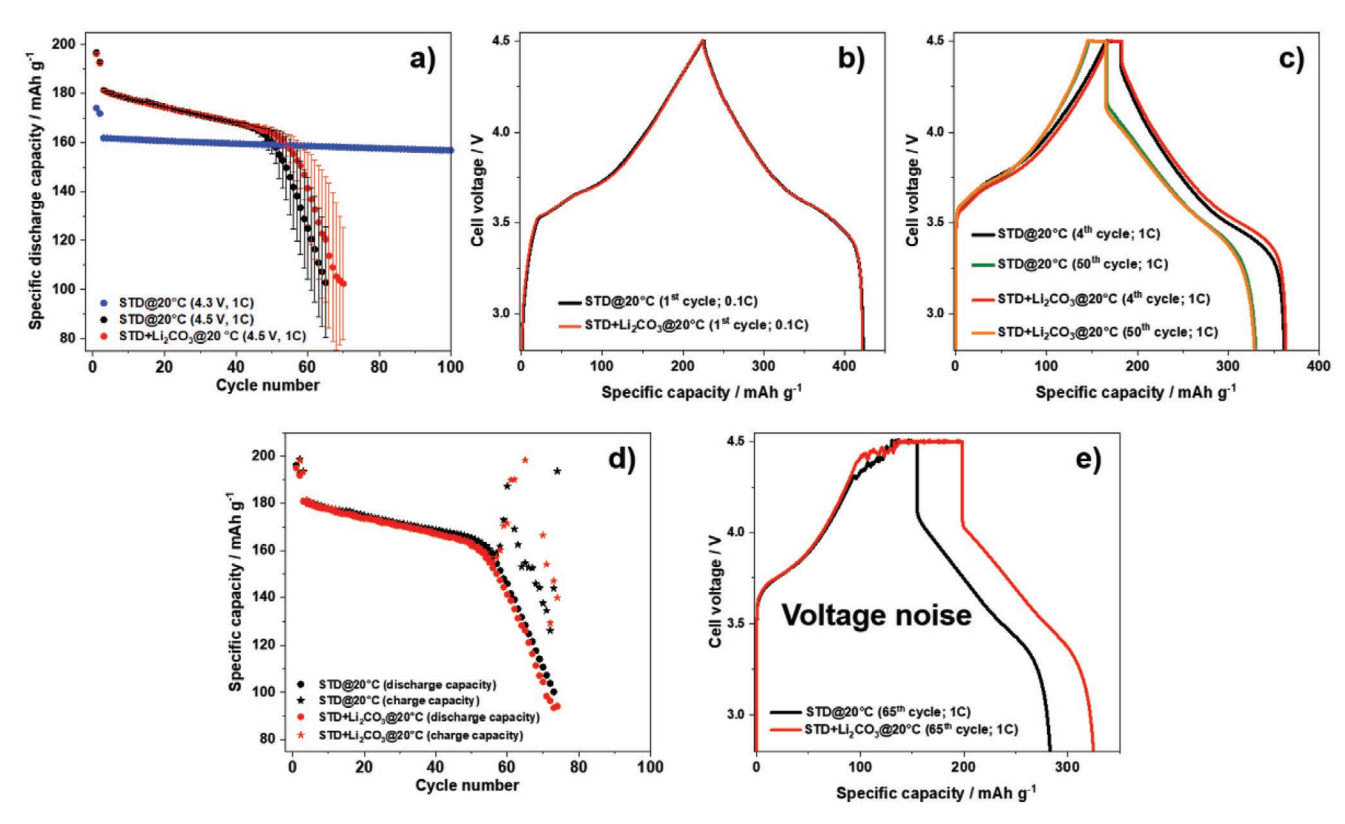
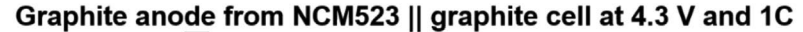
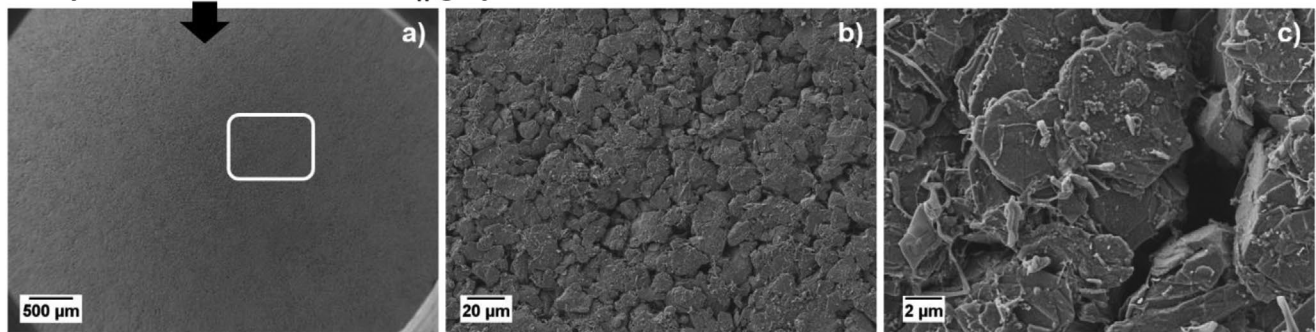


Figure 1. a) Comparison of the charge/discharge cycling performance of NCM523 || graphite full-cells (coin cells, two-electrode configuration) in cell voltage ranges of 2.8–4.3 and 2.8–4.5 V using the standard electrolyte ('STD@20 °C'; 1 M LiPF<sub>6</sub> in EC:EMC 3:7) and the STD electrolyte with 1 wt% Li<sub>2</sub>CO<sub>3</sub> stored at 20 °C for 3 days ('STD+Li<sub>2</sub>CO<sub>3</sub>@20 °C'). b,c) Cell voltage profiles of selected cycles of the cells operated at 4.5 V before the 'rollover' failure, d) charge and discharge capacities during cycling of one representative cell operated at 4.5 V and e) cell voltage profiles of the 65th cycle (within the 'rollover' failure) of the cells operated at 4.5 V.





## Graphite anode from NCM523 || graphite cell at 4.5 V and 1C

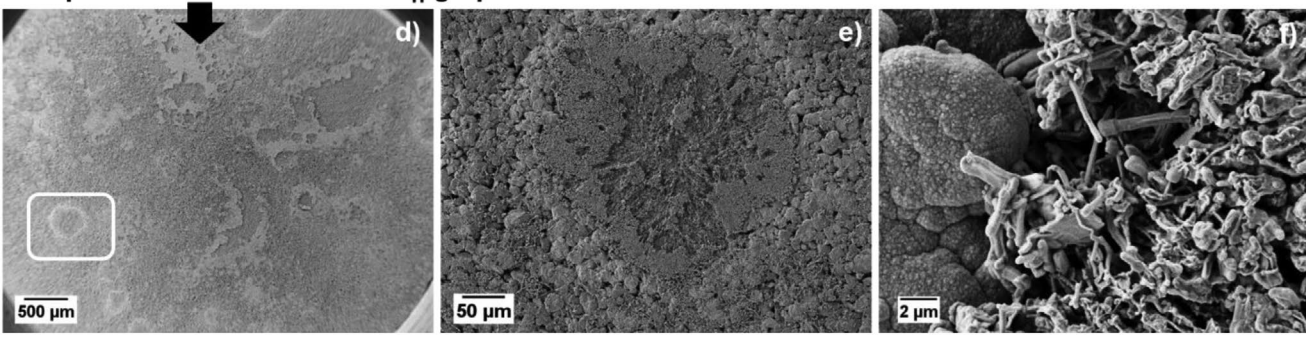


Figure 2. SEM images of the graphite anode after 100 charge/discharge cycles in NCM523 || graphite full-cells (coin cells, two-electrode configuration; see Figure 1a) in cell voltage ranges of a−c) 2.8−4.3 V and d−f) 2.8−4.5 V, both using the 'STD@20 °C' electrolyte.

and without  $\text{Li}_2\text{CO}_3$  additive result in a nearly identical performance (Figure 1a). The comparison of the charge/discharge cell voltage profiles confirms that  $\text{Li}_2\text{CO}_3$  has no significant effect, as the profiles are almost overlapping (Figure 1b,c). The strong charge spikes within the rollover failure and the corresponding voltage noise of both cells demonstrate that both electrolytes result in the formation of (micro-)short-circuits (Figure 1c,d). As shown in previously, [11,17] the presence of voltage noise is an indicator for the penetration of Li metal dendrites through the separator thereby leading to short-circuits by reaching the cathode.

The SEM images of the graphite anodes from 4.3 V cells (Figure 2a-c) do not show any obvious thick deposits (SEI formation) after 100 cycles, even though a small amount of Li metal dendrites in the form of needles is visible (Figure 2c). In contrast, the graphite surface from the cell cycled at 4.5 V depicts broad and thick deposits, which mainly appear as large 'islands' surrounded by a grey film (Figure 2d-f). These islands can be identified as Li metal dendrites (Figure 2f), whereas the grey film surrounding the dendrites can be identified as highly covered graphite particles, that is, covered with thick deposits most likely due to significant SEI growth. Further explanations can be found in our previous work.[11] To verify the negligible effect of the Li<sub>2</sub>CO<sub>3</sub> additive with respect to TM deposition and Li metal dendrite formation at graphite, the graphite anode from the cell using the 'STD+Li<sub>2</sub>CO<sub>3</sub>@20 °C' electrolyte was analyzed via SEM-EDX studies after 100 cycles. The impact of the 'STD@20 °C' electrolyte on TM deposition and Li metal dendrite formation has been discussed previously.[11] A

photograph of the harvested graphite anode (**Figure 3**a) displays strong metallic shiny depositions at the surface. These shiny depositions can be seen as a bright grey film at the anode via SEM (Figure 3b), which were identified as Li metal dendrites (Figure 3c). Especially, at the same positions where these thick Li metal dendrites can be found, a high accumulation of the three TMs Ni, Co, and Mn was found by EDX, as in Figure 3d, 3e, and 3f). These observations confirm that  $\text{Li}_2\text{CO}_3$  as additive, that is, when stored in the carbonate-based electrolyte at 20 °C, has no significant effect with respect to TM deposition and Li metal formation.

# 2.2. Prevention of Rollover Failure by Li<sub>2</sub>CO<sub>3</sub>-Based Electrolyte Stored at 40°C

In a second approach, 1 wt% of  $\rm Li_2CO_3$  was stored for 3 days in the carbonate-based electrolyte at 40 °C ('STD+Li\_2CO\_3@40 °C'). We noted a high solubility of  $\rm Li_2CO_3$ , because of the slightly higher temperature. The motivation for the 40 °C storage experiment was to examine the effect of a moderate temperature during electrolyte preparation on the cell performance. It is not uncommon that laboratories without air conditioning can easily reach temperatures up to  $\approx 35$  °C or even more during hot summer periods, which in turn has an impact on the quality of stored electrolytes. Additionally, in the case of electrolyte delivery from the supplier to the consumer, it might also be difficult to ensure a constant temperature, for example, of 20 °C or below, during the complete transport.

www.advancedsciencenews.com www.advenergymat.de

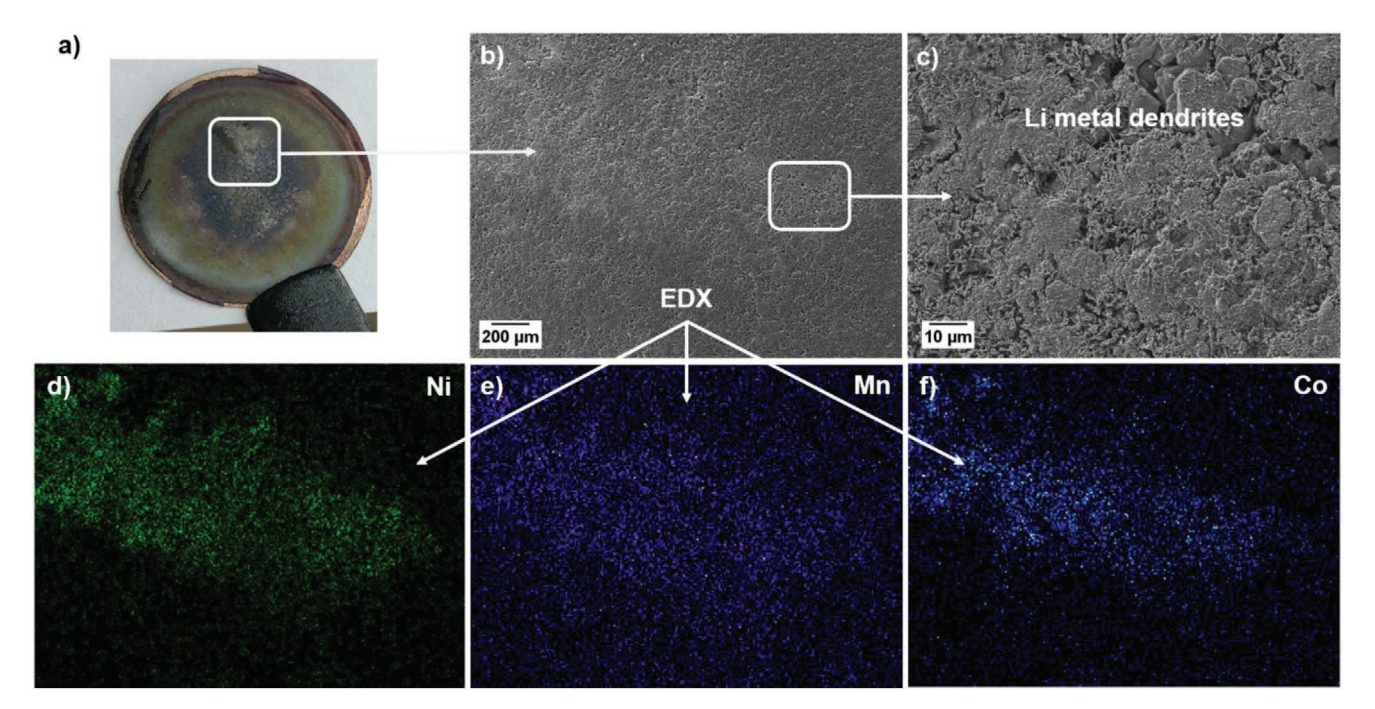


Figure 3. a) Photograph of the graphite anode after 100 charge/discharge cycles in NCM523  $\parallel$  graphite full-cells operated at 2.8–4.5 V (coin cells, two-electrode configuration; see Figure 1a) using the 'STD+Li<sub>2</sub>CO<sub>3</sub>@20 °C' electrolyte; b,c) Corresponding SEM images of the graphite anode and d–f) EDX elemental mappings of Ni (d), Mn (e), and Co (f) from the SEM image in part (b).

After storage at 40 °C, the 'STD+Li<sub>2</sub>CO<sub>3</sub>@40 °C' electrolyte was evaluated in the same cell setup as before, that is, in NCM523 || graphite full-cells operated at 20 °C and 2.8-4.5 V. To exclude that the storage experiment at 40 °C itself (without Li<sub>2</sub>CO<sub>3</sub>) results in a performance improvement, for example, due to LiPF<sub>6</sub> decomposition products at elevated temperature, [18] both electrolytes (with/without Li2CO3) were stored at 40 °C and compared in terms of their electrochemical performance (Figure 4). The STD electrolyte without Li<sub>2</sub>CO<sub>3</sub> additive, which was stored at 40 °C ('STD@40 °C'), does not lead to any improvement of the cycling performance (Figure 4a), which also indicates that 40 °C storage does result in any significant changes of the electrolyte (see <sup>19</sup>F NMR spectra, Figure S1, Supporting Information), that is, in formation of beneficial electrolyte decomposition products, acting as functional electrolyte additive(s).

In contrast, the 'STD+Li $_2$ CO $_3$ @40 °C' electrolyte results in a significant performance improvement of the NCM523  $\parallel$  graphite cells with a capacity retention of  $\approx$ 95% after 100 cycles. The graphite anodes were collected for both electrolyte formulations after 100 cycles to analyze TM deposition and Li metal dendrite formation at the anode surface (Figure 4c–f). The images of the aged graphite anode using the 'STD@40 °C' electrolyte show thick island-like depositions, which were identified as Li metal dendrites (Figure 4c,d) which agrees with the results observed for the 'STD@20 °C' and 'STD+Li $_2$ CO $_3$ @20 °C' electrolytes (stored at 20 °C; Figures 2d–f and 3).

The images of the aged graphite anode from the cell using the 'STD+Li<sub>2</sub>CO<sub>3</sub>@40 °C' electrolyte display is a more or less smooth and clean anode surface without any significant thick shiny deposits (Figure 4e,f), showing no Li metal dendrite formation. Similar to cells based on electrolytes stored at 20 °C

(Figure 1d,e), the cells using the 'STD@40 °C' electrolyte resulted in voltage noise, indicating the presence of (micro-) short-circuits (Figure 4b). In contrast, the 'STD+Li $_2$ CO $_3$ @40 °C' electrolyte prevents the formation of Li metal dendrites, thus the voltage noise behavior (Figure 4a,b).

These findings suggest that the Li<sub>2</sub>CO<sub>3</sub> additive can prevent TM deposition at graphite, which is known to induce Li metal formation. To verify this assumption, laser ablation-inductively coupled plasma-mass spectrometry (LA-ICP-MS) analyses of delithiated graphite anodes were performed,[19] allowing an elemental mapping of the whole anode and detecting the elements Li, Ni, Co, and Mn. Thereby, the anodes from full-cells at 4.3 (Figure 5a-d) and 4.5 V (Figure 5e-h), both using 'STD@20 °C', were compared to the anodes from full-cells at 4.5 V utilizing 'STD+Li<sub>2</sub>CO<sub>3</sub>@40 °C' (Figure 5i–l). The anode cycled at 4.3 V in 'STD@20 °C' shows a relatively low accumulation of lithium, even though few spots with higher intensity can be found, indicating Li metal formation (Figure 5a). In contrast, the graphite anode cycled at 4.5 V using 'STD@20 °C' shows a high accumulation of lithium, mostly island-like agglomerated, indicated by the highest intensity (red) at the surface (Figure 5e). These island-like deposits were identified as Li metal dendrites (Figures 3 and 4). Especially at the positions of the Li metal dendrite islands and their surroundings, a high accumulation of the three TMs (Ni, Co, and Mn) were found (Figure 5f,g,h), similar to our previous results obtained via SEM/EDX studies. Thereby, Mn shows a more broadly distribution and an overall higher intensity over the anode surface compared to Ni and Co deposits (Figure 5h). These results correlate well with the findings from the anode cycled at 4.3 V, that is, a reduced accumulation of lithium and Mn and nearly no detection of Ni and Co at the graphite surface (Figure 5a-d).

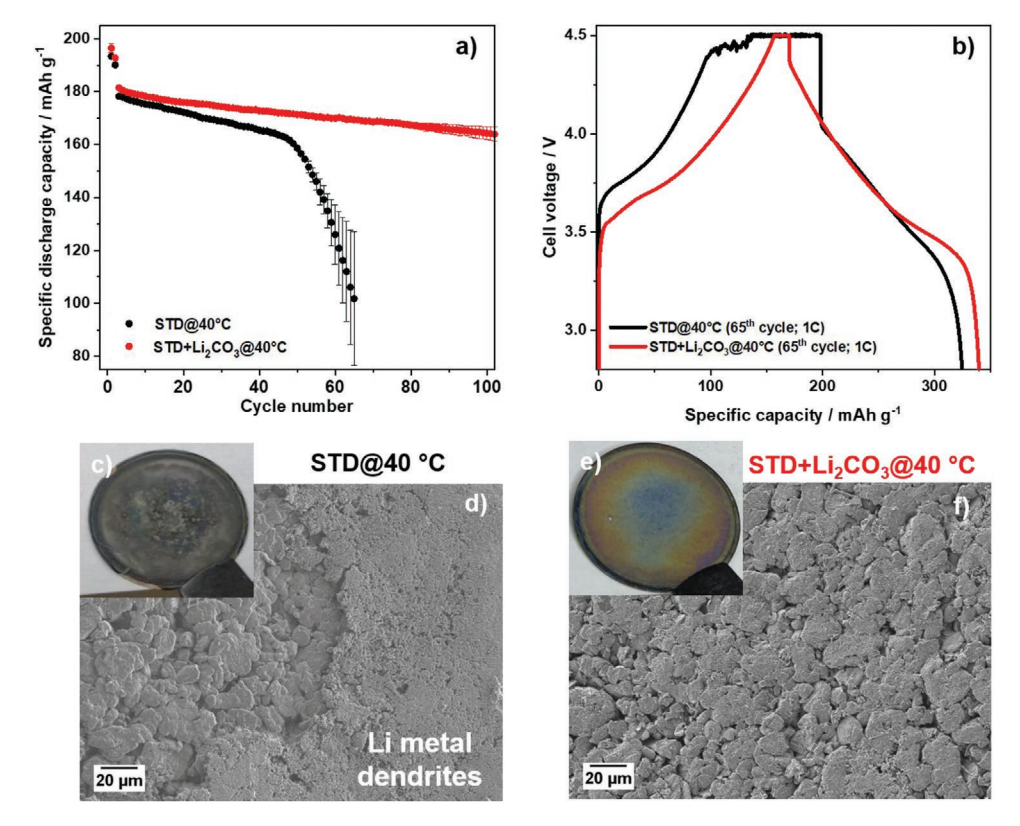


Figure 4. a) Comparison of the charge/discharge cycling performance of NCM523  $\parallel$  graphite full-cells (coin cells, two-electrode configuration) in a cell voltage range of 2.8–4.5 V using the 'STD@40 °C' electrolyte and the 'STD+Li<sub>2</sub>CO<sub>3</sub>@40 °C' electrolyte; b) Cell voltage profiles of the 65th cycle (within the 'rollover' failure); c,d) Photograph and SEM image of the graphite anode after 100 cycles using the 'STD@40 °C' electrolyte; e,f) Photograph and SEM image of the graphite anode after 100 cycles using the 'STD+Li<sub>2</sub>CO<sub>3</sub>@40 °C' electrolyte.

The anode from the 4.5 V cells using 'STD+Li<sub>2</sub>CO<sub>3</sub>@40 °C' electrolyte displays no formation of thick lithium 'islands' at the electrode surface (Figure 5i), as only a low intensity of lithium was detected, despite few lithium spots with higher intensity, similar to the cells operated at 4.3 V (Figure 5a). We assume that these minor lithium amounts over the complete anode can be attributed to lithiated graphite particles, as the cycling was performed at 1C. A very homogeneous distribution of Mn with low intensity can be found over the complete anode (Figure 51), indicating that parts of the lithium amounts can be the initial Li metal dendrites, which could hardly be identified via SEM. Nevertheless, the most important observation is that only a negligible amount of Ni and Co is found at the anode surface (Figure 5j,k). These findings confirm that the use of Li<sub>2</sub>CO<sub>3</sub> as 'additive' in the carbonate-based electrolyte, that is, when stored at 40 °C, results in an effective suppression of the Ni and Co deposition and reduced Mn deposition at the graphite anode in LIB full-cells operated at 4.5 V. It must be noted that Mn deposition at graphite even occurs during operation at 4.3 V (Figure 5d) and cannot be completely suppressed by use of Li<sub>2</sub>CO<sub>3</sub> as 'additive' at 4.5 V (Figure 5l), in contrast to Ni and Co deposition at graphite. In our previous work,[11] we also noticed that the severe 'rollover' failure mechanism of high-voltage NCM523 || graphite cells is primarily initiated by significant Mn deposition at graphite. In this respect, Manthiram and coworkers reported on the performance of NCM811 || graphite cells and found that Mn appears to have a higher susceptibility

towards dissolution compared to Ni and Co for a high-voltage operation at  $\geq$  4.4  $V_{\rm c}^{\rm [9g]}$ 

#### 2.3. In Situ Formation of Lithium Difluorophosphate

It can be assumed that  $\text{Li}_2\text{CO}_3$  reacts already at  $\approx$ 40 °C and forms a beneficial new electrolyte additive by reactions with the electrolyte components. Lucht and co-workers demonstrated that the presence of  $\text{Li}_2\text{CO}_3$  in a carbonate-based LiPF<sub>6</sub>-containing electrolyte (i.e., in dimethyl carbonate, DMC) results in a dark brownish electrolyte when stored at 55 °C after 2 days, which indicated significant promotion of electrolyte degradation. They found that  $\text{Li}_2\text{CO}_3$  reacts with LiPF<sub>6</sub> to form LiF, CO<sub>2</sub>, and LiDFP (F<sub>2</sub>PO<sub>2</sub>Li) at 55 °C, according to Equation (1):

$$LiPF_6 + 2Li_2CO_3 \rightarrow F_2PO_2Li + 2CO_2 + 4LiF$$
 (1)

We found no tangible publication in which the reaction of  $\text{Li}_2\text{CO}_3$  with  $\text{LiPF}_6$  was described to occur at a moderate temperature of \$\approx40\ ^{\circ}\$C, which we believe is of great importance, as a slight temperature increase of the electrolyte, for example, to \$\approx35-40\ ^{\circ}\$C can easily occur during electrolyte preparation, storage, or transport. We analyzed the carbonate-based electrolytes with  $\text{Li}_2\text{CO}_3$  (at 20 and 40 ^{\circ}\$C) and without  $\text{Li}_2\text{CO}_3$  (at 40 ^{\circ}\$C) by means of anion separated chromatography after 3 days of storage. Considering that the 'STD+Li<sub>2</sub>CO<sub>3</sub>@40 ^{\circ}\$C' electrolyte

\_\_\_\_\_ /MAIERIALS

www.advancedsciencenews.com www.advenergymat.de

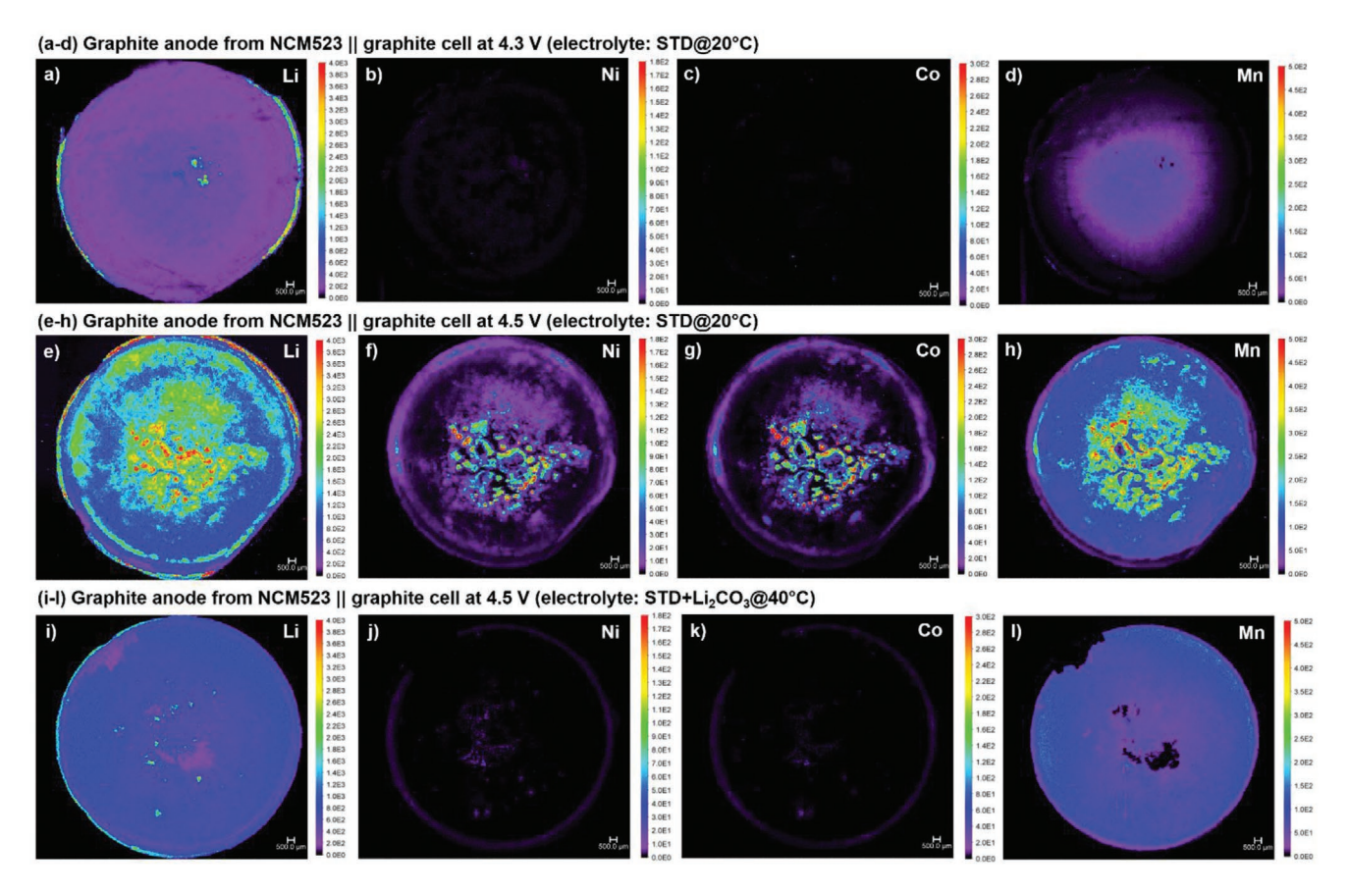


Figure 5. LA-ICP-MS analysis of the graphite anodes (Ø15 mm discs) after 100 charge/discharge cycles in NCM523  $\parallel$  graphite full-cells (coin cells, two-electrode configuration). a–d) Cells were operated at 4.3 V using the 'STD@20 °C' electrolyte; e–h) Cells were operated at 4.5 V using the 'STD#20 °C' electrolyte; i–l) Cells were operated at 4.5 V using the 'STD+Li2CO3@40 °C' electrolyte. The following elements have been analyzed: (a,e,i) Li; (b,f,j) Ni; (c,g,k) Co; (d,h,l) Mn. A high/low intensity of each element can be identified via the color code, that is, from low intensity to high intensity: violet (lowest intensity), blue, green, yellow, red (highest intensity).

did not show any significant color change after storage at 40 °C, in comparison to the work of Lucht and co-workers, [ $^{20a}$ ] it is not obvious that the  $\text{Li}_2\text{CO}_3$  might already be completely consumed during electrolyte preparation at 40 °C.

As shown in the anion chromatogram (Figure 6a), only a negligible amount of fluoride and difluorophosphate is found for 'STD@40 °C' (black curve), indicating that the storage at 40 °C has no significant impact on electrolyte degradation. Similar amounts of difluorophosphate were found for the 'STD+Li<sub>2</sub>CO<sub>3</sub>@20 °C' electrolyte (orange curve). The only difference is that the fluoride signal completely disappeared, which can be attributed to the reaction of Li<sub>2</sub>CO<sub>3</sub> with residues of HF in the electrolyte, which will generate CO2, LiF, and H2O.[21] These results are supported by <sup>19</sup>F-NMR analyses (Figure S1, Supporting Information). These results also explain the similarity of the cycling performance of NCM523 || graphite cells using either 'STD@40 °C' (Figure 4a) or 'STD+Li<sub>2</sub>CO<sub>3</sub>@20 °C' electrolytes (Figure 1a). In contrast, the 'STD+Li<sub>2</sub>CO<sub>3</sub>@40 °C' electrolyte (red curve) revealed the formation of 0.55% difluorophosphate, demonstrating that already moderate temperatures of 40 °C can result in a complete consumption of Li<sub>2</sub>CO<sub>3</sub>, which results in a newly in situ generated electrolyte additive (Figure 6a). To

further verify that the generated amount of difluorophosphate from 'STD+Li<sub>2</sub>CO<sub>3</sub>@40 °C' is the major reason for the beneficial impact of Li<sub>2</sub>CO<sub>3</sub> on the cycling performance of HV-LIB cells, 0.5 wt% LiDFP was added directly to the 'STD@20 °C' electrolyte and evaluated in NCM523 || graphite full-cells (Figure 6b). In general, we found that the addition of higher amounts of Li<sub>2</sub>CO<sub>3</sub> to the electrolyte (i.e., >1 wt%) will result in the formation of higher amounts of LiDFP when stored at 40 °C. In comparison to the work of Lucht and co-workers, [20a] we also stored the electrolyte with 1 wt% Li2CO3 at 55 °C (for 4 days) and found an even higher amount of 0.75 wt% LiDFP. However, we could not observe any color change of the electrolyte after storage, which could indicate significant electrolyte degradation. In summary, higher amounts of Li<sub>2</sub>CO<sub>3</sub> as well as elevated temperatures (≥40 °C) enable an increased formation of LiDFP. Nevertheless, we only focused on the addition of 1 wt% Li<sub>2</sub>CO<sub>3</sub> and 40 °C storage for the following mechanistic investigation.

Both NCM523 || graphite cells, using the LiDFP additive (green curve) as well as the in situ generated LiDFP additive (red curve), show a very similar cycling performance (Figure 6b). The charge/discharge cell voltage profiles of both cells are strongly overlapping and cannot be distinguished, as shown for selected

www.advancedsciencenews.com

www.advenergymat.de

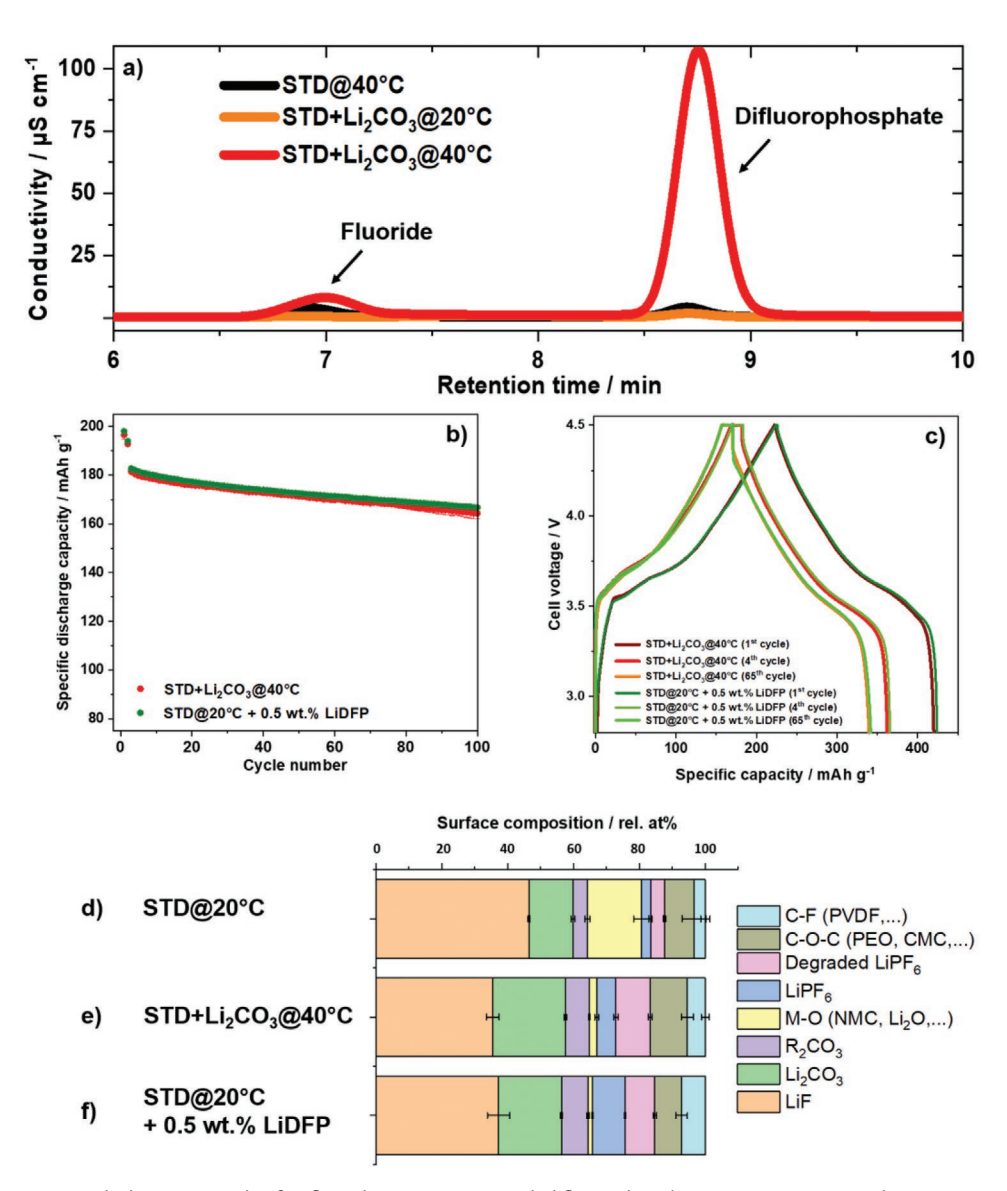


Figure 6. a) Anion separated chromatography for fluoride anions ( $F^-$ ) and difluorophosphate anions ( $F_2PO_2^-$ ). b) Comparison of the charge/discharge cycling performance of NCM523 || graphite full-cells (coin cells, two-electrode configuration) in a cell voltage range of 2.8–4.5 V using the 'STD+Li<sub>2</sub>CO<sub>3</sub>@40 °C' electrolyte and the electrolyte 'STD@20 °C + 0.5 wt% LiDFP'; c) Corresponding cell voltage profiles of selected cycles. d–f) Relative atomic concentrations from XPS analyses of the graphite anode surfaces after 100 charge/discharge cycles in NCM523 || graphite full-cells (coin cells, two-electrode configuration) in a cell voltage range of 2.8–4.5 V using the electrolytes (d) 'STD@20 °C', (e) 'STD+Li<sub>2</sub>CO<sub>3</sub>@40 °C', and (f) 'STD@20 °C + 0.5 wt% LiDFP'.

cycles in Figure 6c. To further verify these results, XPS analyses of the graphite anodes have been performed of full-cells using the electrolytes 'STD@20 °C', 'STD+Li<sub>2</sub>CO<sub>3</sub>@40 °C', and 'STD@20 °C + 0.5 wt% LiDFP' after 100 cycles. The relative atomic concentrations of the surface of the graphite anodes are given in Figure 6d–f. It must be noted that these ratios only provide information about the composition of the top surface of the graphite anodes (information depth of  $\approx 3-10$  nm of XPS) and, thus, about the elemental composition of the measured SEI layer but not absolute amounts of the whole composition in the depth of the electrode or of the SEI. Differences in terms of SEI composition can be clearly observed, that is, an increased amount of LiF and metal-oxide species for

the graphite anodes cycled in 'STD@20 °C' (Figure 6d), while both anodes from electrolyte additive-containing cells display very similar atomic concentrations (Figure 6e,f). The latter anodes display enhanced concentrations of  $\text{Li}_2\text{CO}_3$  and  $\text{R}_2\text{CO}_3$  species, and an increased amount of degraded LiPF<sub>6</sub> within the SEI, while the amounts of LiF and metal-oxide species are significantly reduced. These findings are further supported when analyzing the P 2p core spectra (Figure S2, Supporting Information), indicating formation of fluorophosphate species ( $\approx 134.1 \text{ eV}$ ) for both additive-containing electrolytes. Other phosphate species (i.e., with lower fluorine content;  $\approx 133.3 \text{ eV}$ ) are found for the 'STD@20 °C' electrolyte (Figure S2, Supporting Information).

www.advancedsciencenews.com

www.advenergymat.de

#### 2.4. Scavenging Mechanism of Transition Metal Cations

The mechanism for the significant prevention of Co and Ni deposition at graphite by in situ formed LiDFP is not clear yet. Li et al. demonstrated that the use of LiDFP resulted in a significant improvement in LiNi<sub>0.55</sub>Co<sub>0.15</sub>Mn<sub>0.3</sub>O<sub>2</sub> || graphite full-cells at 4.45 V and at room temperature, whereby the additive-free cell resulted in rollover failure after ≈120 cycles.<sup>[22]</sup> They attributed the beneficial impact of LiDFP to modified interphases at both the cathode and anode. Kim et al. investigated a combination of LiDFP and vinylene carbonate as additives in graphite | Li metal cells and observed that LiDFP was reduced at higher cell voltages than ethylene carbonate, resulting in a beneficial P-O rich SEI layer at graphite.<sup>[23]</sup> Additionally, Wang et al. investigated LiDFP as additive in NCM111 | graphite cells operated at 4.5 V and observed that a rollover failure was impeded, due to prevention of TM deposition at the anode. [13a] However, the authors could not unravel the underlying mechanism.<sup>[13a]</sup> Zhao et al. reported on LiNi<sub>0.5</sub>Mn<sub>0.25</sub>Co<sub>0.25</sub>O<sub>2</sub>  $\parallel$  Li metal cells using LiDFP as additive and postulated that small amounts of difluorophosphate undergo electrochemical side reactions, resulting in the formation of LiF and Li<sub>3</sub>PO<sub>4</sub>, according to Equation (2).[24]

$$2H_2O + PO_2F_2^- + 4Li^+ \rightarrow Li_3PO_4 + LiF + HF + 3H^+$$
 (2)

Many researchers found significant amounts of phosphates within the SEI layer at the anode after cycling when studying

LiDFP as additive. [22-24] To clarify the role of these phosphates, that is, lithium phosphate (Li<sub>3</sub>PO<sub>4</sub>), with respect to the improved cycling performance and prevention of TM deposition at the anode, we performed the following experiments: We found that ≈250 ppm Li<sub>3</sub>PO<sub>4</sub> can be dissolved in 'STD@20 °C'. To elaborate the interaction of Li<sub>3</sub>PO<sub>4</sub> and dissolved Ni<sup>2+</sup> and Co<sup>2+</sup> cations, Ni(TFSI)<sub>2</sub> and Co(TFSI)<sub>2</sub> were each dissolved in 'STD@20 °C'. Afterwards, Li<sub>3</sub>PO<sub>4</sub> was added to the electrolyte and left for 24 h. Thereafter, the electrolyte and the precipitated solids were separated by filtration (Figure 7). Initially, the Co<sup>2+</sup>-containing electrolyte displayed a pink color, while the addition of Li<sub>3</sub>PO<sub>4</sub> resulted in a strong color change, that is, from pink to colorless (Figure 7c), and a precipitation of a violet (Co-containing) solid (Figure 7d). Analogously, the Ni<sup>2+</sup>-containing electrolyte displayed a light green/yellow color, and the addition of Li<sub>3</sub>PO<sub>4</sub> resulted in a colorless electrolyte (Figure 7a) and precipitation of a yellow to greenish (Ni-containing) solid (Figure 7b). We believe that the solid residues can be attributed to the formation of the insoluble Co<sub>3</sub>(PO<sub>4</sub>)<sub>2</sub> (violet color) and Ni<sub>3</sub>(PO<sub>4</sub>)<sub>2</sub> (yellow to greenish color). Further, we analyzed the electrolyte after filtration by means of cation separated chromatography. The initial concentrations of Ni<sup>2+</sup> or Co<sup>2+</sup> were ≈800 ppm in the initially prepared 'STD@20 °C' electrolytes (Figure 7e). After 24 h in presence of Li<sub>3</sub>PO<sub>4</sub>, the Ni<sup>2+</sup> and Co<sup>2+</sup> concentrations dropped below the limit of quantification (≤7.5 ppm), which supports the proposed mechanism for cation 'scavenging' of phosphate species. The same experiment was performed to clarify the impact of Li<sub>3</sub>PO<sub>4</sub> on 'scavenging' of manganese cations: Mn(TFSI)<sub>2</sub>

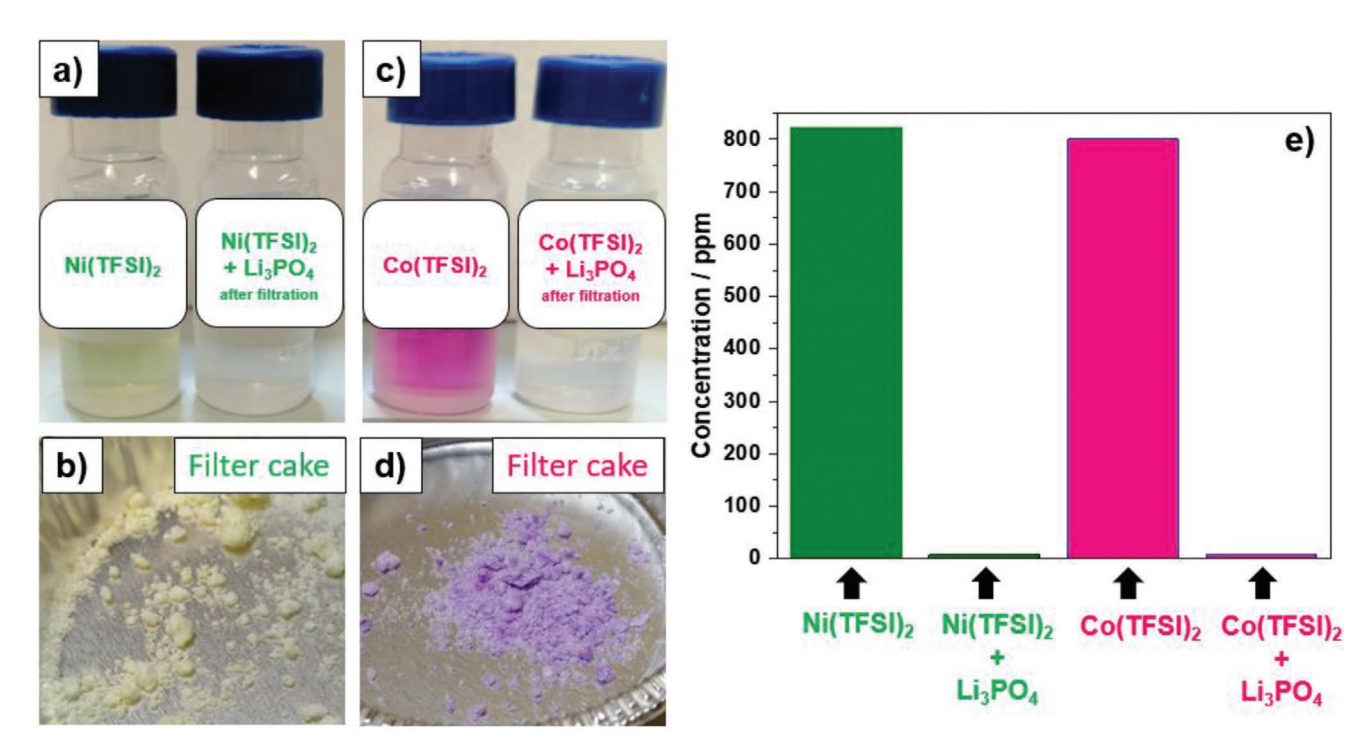


Figure 7. a,b) Photographs of (a) the 'STD@20 °C (1 mL) + 10 mg Ni(TFSI)<sub>2</sub> (800  $\pm$  3 ppm Ni<sup>2+</sup> ions)' electrolyte (left) and the 'STD@20 °C (1 mL) + 10 mg Ni(TFSI)<sub>2</sub> + 100 mg Li<sub>3</sub>PO<sub>4</sub>' electrolyte after 24 h and after filtration (right) and b) of the separated precipitated solids ('filter cake') from the Ni(TFSI)<sub>2</sub>-containing electrolyte. c,d) Photographs of (c) the 'STD@20 °C (1 mL) + 10 mg Co(TFSI)<sub>2</sub> (800  $\pm$  1 ppm Co<sup>2+</sup> ions)' electrolyte (left) and the 'STD@20 °C (1 mL) + 10 mg Co(TFSI)<sub>2</sub> + 100 mg Li<sub>3</sub>PO<sub>4</sub>' electrolyte after 24 h and after filtration (right) and d) of the separated precipitated solids ('filter cake') from the Co(TFSI)<sub>2</sub>-containing electrolyte. e) Results from cation separated chromatography for Ni<sup>2+</sup> and Co<sup>2+</sup> cations from electrolytes from (a) and (c). After addition of Li<sub>3</sub>PO<sub>4</sub>' Ni<sup>2+</sup> and Co<sup>2+</sup>  $\leq$  7.5 ppm (= limit of quantification).

ADVANCED ENERGY MATERIALS

was dissolved in 'STD@20 °C' and  $\text{Li}_3\text{PO}_4$  was added (storage for 24 h). After 24 h, the Mn²+ concentration also dropped below the limit of quantification ( $\leq$ 7.5 ppm). As the electrolyte and the precipitated solids were colorless, we did not include the corresponding photographs.

We believe that besides the electrolyte additive's role in the formation of beneficial interphases at the anode and/or cathode, it is also very important to investigate the additive's impact on the in situ formation of possible decomposition products, which in turn may significantly influence the TM deposition behavior at graphite anodes. Phosphates, such  $\text{Li}_3\text{PO}_4$  or  $\text{LiPO}_2\text{F}_2$ , have been shown to effectively act as 'scavenging' agents for  $\text{Ni}^{2+}$  and  $\text{Co}^{2+}$  cations. Therefore, also the beneficial

impact of inorganic surface coatings for NCM cathode materials (e.g.,  $\text{Li}_3\text{PO}_4$ )<sup>[25]</sup> should be reconsidered and systematically evaluated in future studies, as such coatings might be able to in situ form insoluble TM products, which cannot cross over to the anode, thus, hindering SEI alteration. Moreover, the impact of the additive concentration (i.e.,  $\text{Li}_2\text{CO}_3$  and/or LiDFP) on the scavenging ability for TM cations should be investigated in future works to achieve further performance gains of high-voltage NCM  $\parallel$  graphite cells.

In particular, the effective scavenging of Mn<sup>2+</sup> cations seems to be critical, as high amounts of Mn are found at the graphite anode under high-voltage operation conditions, which induces subsequent SEI growth, Li metal dendrite formation, and the

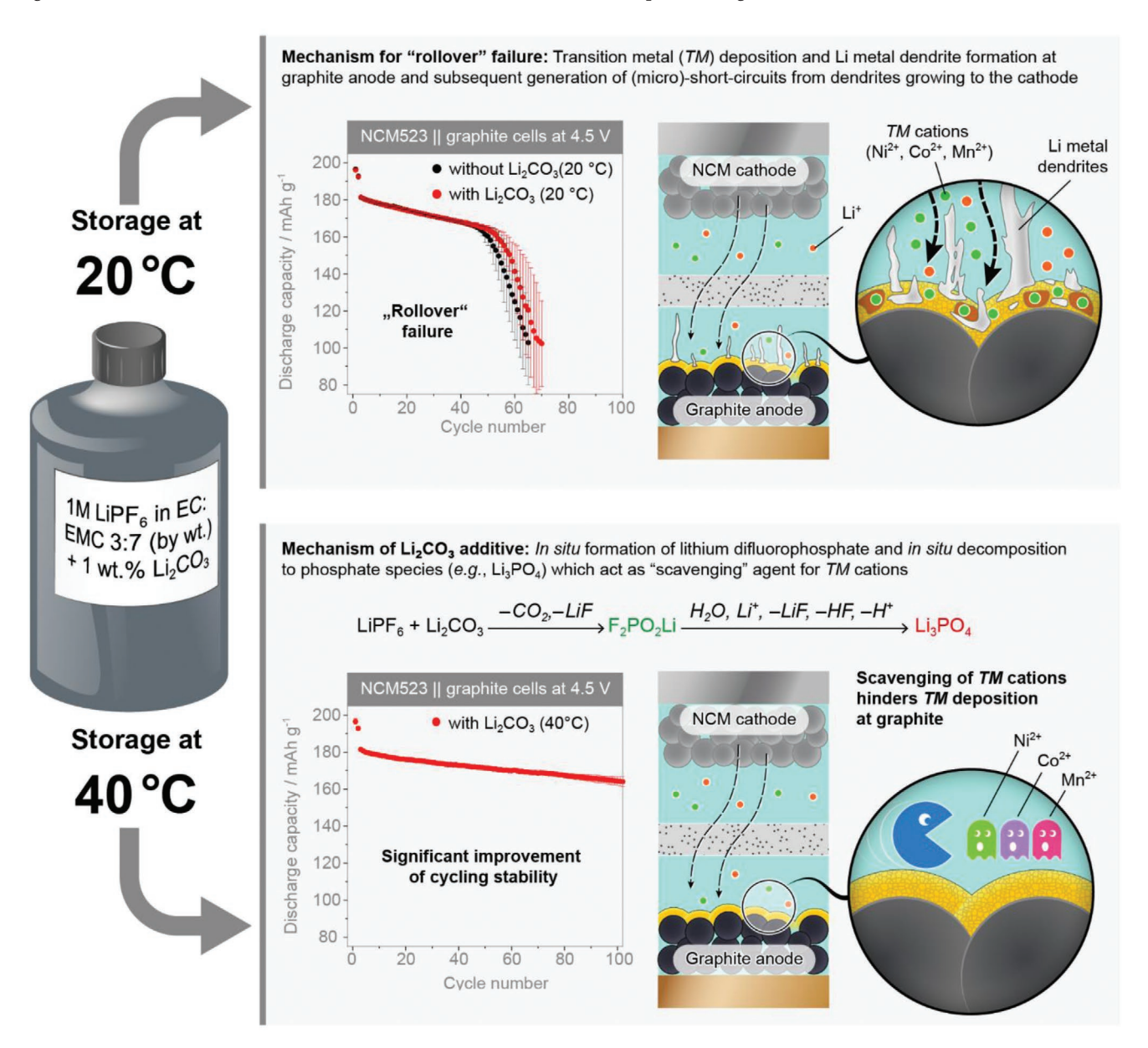


Figure 8. Schematic illustration of the underlying mechanism of the  $Li_2CO_3$  additive in the carbonate-based electrolyte, hindering the 'rollover' failure of NCM523  $\parallel$  graphite cells operated at 2.8–4.5 V. Lithium difluorophosphate ( $F_2PO_2Li$ , LiDFP) is formed within the electrolyte during storage at 40 °C. In situ formed decomposition species of LiDFP (e.g.,  $Li_3PO_4$ ) act as 'scavenging' agents for TM cations, thus, significantly reducing TM deposition at the graphite anode, which would subsequently result in an Li metal deposition and dendrite growth.

www.advancedsciencenews.com www.advenergymat.de

ADVANCED ENERGY MATERIALS

severe 'rollover' failure.<sup>[11]</sup> In future works, one should also focus on the analysis of the NCM cathode, as the electrolyte formulation might result in significant transformations of the NCM cathode (sub)surface structure during high voltage operation. As shown in literature, such cathode surface alterations might lead to enhanced TM dissolution,<sup>[26]</sup> which in turn could have an impact on the 'rollover' failure.

#### 3. Conclusion

NCM523 || graphite cells operated at 4.5 V suffer from severe capacity fading, known as 'rollover' failure, caused by TM deposition (Ni, Mn, Co), significant SEI growth and Li metal dendrite formation at the anode, and subsequent generation of (micro-)short-circuits (Figure 8). Here, we elucidated the beneficial effect of Li<sub>2</sub>CO<sub>3</sub> as additive in a carbonate-based electrolyte with respect to its ability to prevent extensive deposition of TMs (in particular Ni and Co) at graphite, consequently impeding this cell failure. Interestingly, the positive impact on cell performance was only observed when the electrolyte was stored at a moderate temperature of 40 °C, while no significant impact was detected when stored at 20 °C. We want to point out that temperatures of 35-40°C can easily be reached during transport/shipping or storage of electrolytes in hot summer periods, which might result in an alteration of the electrolyte components.

We were able to unravel the underlying mechanism and the role of Li<sub>2</sub>CO<sub>3</sub>: Li<sub>2</sub>CO<sub>3</sub> reacts with the LiPF<sub>6</sub> salt during storage at 40 °C and in situ forms LiDFP. These findings are of great importance, as studies of novel electrolyte formulations can be easily influenced by temperature effects and possible alteration of the electrolyte components, which in turn influences cell performance. LiDFP was able to significantly prevent the deposition of Ni and Co species at the graphite anode, and subsequently impeded the rollover cell failure. To further clarify the role of LiDFP, we elaborated a literature-known decomposition product of LiDFP, that is, Li<sub>3</sub>PO<sub>4</sub>, which was shown to be formed during electrochemical operation. Li<sub>3</sub>PO<sub>4</sub> plays an important role in the prevention of Ni and Co deposition at the anode, as it acts as 'scavenging' agent for Ni<sup>2+</sup> and Co<sup>2+</sup> ions, forming insoluble compounds, thus, significantly reducing TM crossover to the anode (Figure 8). In summary, LiDFP can be considered as highly promising electrolyte additive for HV-LIB cells. In this context, the functionality of inorganic coatings for cathode materials (e.g., Li<sub>3</sub>PO<sub>4</sub>)<sup>[25a]</sup> should be reconsidered, as such coatings might be able to form hardly soluble TM compounds, which thus cannot dissolve, crossover, and induce severe SEI alteration at the graphite anode.

## 4. Experimental Section

Electrode Preparation: NCM523-based cathodes and graphite-based anodes were prepared in a large-scale at an in-house battery line. The cathodes consisted of 95 wt% NCM523 (pristine NCM523; Custom Cells Itzehoe GmbH), 3 wt% polyvinylidene difluoride (PVdF) binder (Solef 5130, Solvay), and 2 wt% carbon black (Super C65, Imerys Graphite & Carbon) and were cast onto aluminum foil (15 µm; Nippon Foil). The used solvent was N-methyl-2-pyrrolidone (NMP, Sigma Aldrich,

purity: 99.5%). The cathode mass loading was 12.2 mg cm $^{-2}$  and the cathode areal capacities were 2.0 mAh cm $^{-2}$  at a cell voltage of 4.3 V and 2.2 mAh g $^{-1}$  at 4.5 V. The anodes consisted of 95 wt% graphite (SG3, natural graphite, SGL Carbon), 1.5 wt% styrene-butadiene-rubber (SBR; SB5521, LIPATON, Polymer Latex GmbH), 3 wt% Na-CMC (Walocel CRT 2000 PPA12; Dow Wolff Cellulosics), and 0.5 wt% carbon black (Super C65, Imerys Graphite & Carbon) and were cast onto copper foil (10  $\mu m$ ; Nippon Foil), using deionized water as solvent. The anode mass loading was 8.8 mg cm $^{-2}$ . After drying and calendaring of the electrode sheets (porosity: 30%), they were punched into circular Ø14 mm (cathode) and Ø15 mm (anode) discs. The electrodes were dried in a vacuum oven at 100 °C under reduced pressure. The electrode capacity balancing of anode and cathode (N:P ratio) was set to  $\approx 1.35 : 1.00$ .

Electrolyte Preparation: The standard electrolyte used in this work was 1 m LiPF $_6$  in ethylene carbonate (EC):ethyl methyl carbonate (EMC) 3:7 (by weight; Solvionic; purity: battery grade), which was either stored at 20 °C (abbreviated as 'STD@20 °C') or stored for 3 days at 40 °C (abbreviated as 'STD@40 °C').

In addition, 1 wt% of Li<sub>2</sub>CO<sub>3</sub> (Sigma Aldrich; CAS No.: 554-13-2; purity: ≥99.0%) was added to the STD electrolyte and stored for 3 days at 20 °C (abbreviated as 'STD+Li<sub>2</sub>CO<sub>3</sub>@20 °C') as well as 40 °C (abbreviated as 'STD+Li<sub>2</sub>CO<sub>3</sub>@40 °C'). Afterwards, the electrolytes were filtered to remove the remaining Li<sub>2</sub>CO<sub>3</sub> in form of a white solid.

In another experiment, 0.5 wt% of the electrolyte additive lithium difluorophosphate (LiDFP; American Elements; CAS No.: 24389-25-1; purity: ≥99.9%) was added to the 'STD@20 °C' electrolyte.

To investigate the interaction of  $\text{Li}_3\text{PO}_4$  and dissolved  $\text{Ni}^{2+}$  and  $\text{Co}^{2+}$  cations, 10 mg of  $\text{Ni}(\text{TFSI})_2$  (Alfa Aesar; CAS No.: 207861-63-0) and 10 mg of  $\text{Co}(\text{TFSI})_2$  (Alfa Aesar; CAS No.: 207861-61-8) were each dissolved in 1 mL of the 'STD@20 °C' electrolyte. From ion chromatography analysis,  $\approx$ 800 ppm of  $\text{Ni}^{2+}$  and  $\text{Co}^{2+}$  were found in the electrolyte. Afterwards, 100 mg of  $\text{Li}_3\text{PO}_4$  (Alfa Aesar; CAS No. 10377-52-3; purity: 99.99%) was added to each of the electrolytes and left for 24 h at 20 °C. The precipitated solids were separated from the electrolyte solution by filtration.

Cell Assembly: 2032-type coin cells (full-cell setup, two-electrode configuration  $^{[27]}$ ) were assembled to investigate transition metal (TM) dissolution from the NCM523 cathode and TM deposition at the graphite anode in NCM523  $\parallel$  graphite full-cells. The Ø15 mm anode disc was separated by a Celgard 2500 separator (polypropylene, one layer) from the Ø14 mm cathode disc, which was soaked with 40  $\mu L$  of the electrolyte.

Constant Current-Constant Voltage Charge/Discharge Cycling: The electrochemical charge/discharge cycling performance of NCM523  $\parallel$  graphite full-cells was studied via constant current (CC) charge/discharge cycling on a Maccor 4000 battery testing system in cell voltage ranges between 2.8–4.3 and 2.8–4.5 V. The cell formation conditions consisted of one cycle at 0.1C and one cycle at 0.2C. Afterwards, the cells were cycled with 1C (1C = 170 mA g<sup>-1</sup> at 4.3 V; 1C = 190 mA g<sup>-1</sup> at 4.5 V). After each charge step, a constant voltage (CV) step was performed with the limiting conditions of either achieving a time limit of maximal 30 min or when the specific current reaches values below 0.05C. All electrochemical studies were performed in climatic chambers at 20 °C. At least three cells were evaluated for each study to ensure a high reproducibility, which is indicated by error bars in the respective figures.

SEM and EDX Investigations of Graphite Anodes After Cycling: The investigation of the surface morphology of the cycled graphite anodes (after 100 cycles) was performed by a Zeiss Auriga electron microscope and EDX was carried out with an accelerating voltage of 20 kV with an energy-dispersive X-ray detector (X-MaxN 80 mm², Oxford Instruments). Prior to analysis, the cells were disassembled in dry atmosphere (dry room) and the anode surfaces were rinsed with 1 mL of EMC. After a short drying period under reduced pressure, the electrodes were transferred into the SEM advice via a vacuum sealed sample holder to avoid any contact to moisture.

LA-ICP-MS Investigations of Graphite Anodes After Cycling: LA-ICP-MS investigations were carried out utilizing a similar procedure as outlined by Schwieters and co-workers and Harte and co-workers. [19,28] The setup



www.advancedsciencenews.com

www.advenergymat.de

**ENERG** 

for all measurements consisted of a 193 nm ArF Excimer laser (Analyte Excite Eximer LA-System, Teledyne Cetac) coupled to a quadrupole based ICP-MS (ICP-MS Agilent 7700 Series, Agilent Technologies). Detailed measurement conditions (ICP parameters, gas flow rates, etc.) are described in the respective literature. In this case, the laser was operated with a spot size of 50  $\mu m$ , 200  $\mu m$  s $^{-1}$  scan speed, shot frequency of 40 Hz, and a fluence of 4 J cm $^{-2}$ , in order to achieve a suitable lateral resolution. For all measurements, the  $^{13}\text{C-signal}$  was used as internal standards to correct for varying ablation yields, transport efficiencies as well as changing plasma conditions during analysis, thus all signals will be given as the  $^{13}\text{C}$  corrected intensities.

XPS Investigations of Graphite Anodes After Cycling: X-ray photoelectron spectroscopy (XPS) samples were mounted on a sample holder and transported to a glovebox connected to an Axis Ultra DLD XPS (Kratos Analytical). From here, samples were moved into an ultra-high vacuum ( $10^{-8}$  mbar) chamber inside the device. Here, samples were stored for at least 12 h to remove volatile species, before moving the samples into the analysis chamber. XPS was measured using a monochromatic Al  $K\alpha$  source ( $h\nu=1486.6$  eV) at an emission current of 10 mA and with an accelerating voltage of 12 kV. A charge neutralizer was used to suppress positive charging of the sample's surface. A small area spectroscopy aperture of 110  $\mu$ m was used for the core spectra of the graphite anodes. The angle of emission was 0° and the hemispherical analyzer was set to a pass energy of 160 eV for survey spectra and 40 eV for graphite anode core spectra. Core spectra were recorded in the following regions: F 1s, O 1s, C 1s, P 2p, and Li 1s.

IC-CD Investigations of Anions and Transition Metal Cations: Ion chromatography (IC) was performed on an 850 Professional IC (Metrohm, Herisau, Switzerland) comprising a chemical suppressor and conductivity detection (CD). A Metrosep A Supp 7- (250  $\times$  4.0 mm, 5  $\mu m$ ; Metrohm) with a Metrosep A Supp 4/5 guard column was used for isocratic anion separation (sodium carbonate/ sodium hydrogen carbonate eluent) at 65 °C and a flow rate of 0.7 mL min^-1 was applied. The developed method is based on Kraft et al. and further parameters and sample preparation were applied according to Henschel et al. [29] Cations were separated on a Metrosep C6-250/4.0 column on a Compact IC Pro 881 instrument (Metrohm, Herisau, Switzerland) with CD. A sample volume of 200  $\mu$ L was separated at 40 °C with an isocratic 0.85 mm oxalic acid/ 4.15 mm nitric acid eluent. The method and sample preparation were based on Vortmann-Westhoven et al. [30] Both IC systems were controlled with MagIC NetTM 3.2.

#### Supporting Information

Supporting Information is available from the Wiley Online Library or from the author.

#### **Acknowledgements**

The authors wish to thank the Federal Ministry for Economic Affairs and Energy (BMWi) for funding this work in the project 'Go3' (03ETE002D). P.H. would like to thank the Ministry of Economic Affairs, Innovation, Digitalization and Energy of the state North-Rhine-Westphalia for funding the 'GrEEn' project (313-W044A). S.v.W. acknowledges the Federal Ministry of Education and Research (BMBF) for funding the project 'Cell-Fill' (03XP0237C). The authors thank the technicians of MEET under the leadership of Pascal Noll for the constant support in view of the production of the electrodes. The authors thank Andre Bar for graphical support.

Open access funding enabled and organized by Projekt DEAL.

#### **Conflict of Interest**

The authors declare no conflict of interest.

# **Data Availability Statement**

Data available on request from the authors.

#### **Keywords**

electrolyte additives, lithium carbonate, lithium difluorophosphate, lithium ion cells, lithium metal plating, rollover failure

Received: December 2, 2020 Revised: December 27, 2020 Published online: January 25, 2021

- [1] a) R. Schmuch, R. Wagner, G. Hörpel, T. Placke, M. Winter, Nat. Energy 2018, 3, 267; b) M. Winter, B. Barnett, K. Xu, Chem. Rev. 2018, 118, 11433; c) X. Zeng, M. Li, D. Abd El-Hady, W. Alshitari, A. S. Al-Bogami, J. Lu, K. Amine, Adv. Energy Mater. 2019, 9, 1900161.
- [2] a) S.-T. Myung, F. Maglia, K.-J. Park, C. S. Yoon, P. Lamp, S.-J. Kim, Y.-K. Sun, ACS Energy Letters 2017, 2, 196; b) Z. P. Cano, D. Banham, S. Ye, A. Hintennach, J. Lu, M. Fowler, Z. Chen, Nat. Energy 2018, 3, 279; c) J. Betz, G. Bieker, P. Meister, T. Placke, M. Winter, R. Schmuch, Adv. Energy Mater. 2019, 9, 1803170.
- [3] a) W. Li, E. M. Erickson, A. Manthiram, *Nat. Energy* 2020, 5, 26;b) A. Manthiram, *Nat. Commun.* 2020, 11, 1550.
- [4] a) D. Andre, S.-J. Kim, P. Lamp, S. F. Lux, F. Maglia, O. Paschos,
  B. Stiaszny, J. Mater. Chem. A 2015, 3, 6709; b) F. Schipper,
  E. M. Erickson, C. Erk, J.-Y. Shin, F. F. Chesneau, D. Aurbach,
  J. Electrochem. Soc. 2017, 164, A6220.
- [5] M. He, C.-C. Su, C. Peebles, Z. Feng, J. G. Connell, C. Liao, Y. Wang, I. A. Shkrob, Z. Zhang, ACS Appl. Mater. Interfaces 2016, 8, 11450.
- [6] H.-H. Ryu, K.-J. Park, C. S. Yoon, Y.-K. Sun, Chem. Mater. 2018, 30, 1155.
- [7] I. Takahashi, H. Kiuchi, A. Ohma, T. Fukunaga, E. Matsubara, J. Phys. Chem. C 2020, 124, 9243.
- [8] a) J. Betz, J.-P. Brinkmann, R. Nölle, C. Lürenbaum, M. Kolek, M. C. Stan, M. Winter, T. Placke, Adv. Energy Mater. 2019, 9, 1900574;
  b) O. C. Harris, S. E. Lee, C. Lees, M. Tang, J. Phys.: Energy 2020, 2, 032002;
  c) W. Li, U.-H. Kim, A. Dolocan, Y.-K. Sun, A. Manthiram, ACS Nano 2017, 11, 5853.
- [9] a) T. Joshi, K. Eom, G. Yushin, T. F. Fuller, J. Electrochem. Soc. 2014, 161, A1915; b) R. Jung, F. Linsenmann, R. Thomas, J. Wandt, S. Solchenbach, F. Maglia, C. Stinner, M. Tromp, H. A. Gasteiger, J. Electrochem. Soc. 2019, 166, A378; c) J. A. Gilbert, I. A. Shkrob, D. P. Abraham, J. Electrochem. Soc. 2017, 164, A389; d) J. Wandt, A. Freiberg, R. Thomas, Y. Gorlin, A. Siebel, R. Jung, H. A. Gasteiger, M. Tromp, J. Mater. Chem. A 2016, 4, 18300; e) C. Zhan, J. Lu, A. Jeremy Kropf, T. Wu, A. N. Jansen, Y. K. Sun, X. Qiu, K. Amine, Nat. Commun. 2013, 4, 2437; f) C. Wang, L. Xing, J. Vatamanu, Z. Chen, G. Lan, W. Li, K. Xu, Nat. Commun. 2019, 10, 3423; g) W. Li, X. Liu, Q. Xie, Y. You, M. Chi, A. Manthiram, Chem. Mater. 2020, 32, 7796.
- [10] a) X. Ma, J. E. Harlow, J. Li, L. Ma, D. S. Hall, S. Buteau, M. Genovese, M. Cormier, J. R. Dahn, J. Electrochem. Soc. 2019, 166, A711; b) R. S. Arumugam, L. Ma, J. Li, X. Xia, J. M. Paulsen, J. R. Dahn, J. Electrochem. Soc. 2016, 163, A2531; c) I. Buchberger, S. Seidlmayer, A. Pokharel, M. Piana, J. Hattendorff, P. Kudejova, R. Gilles, H. A. Gasteiger, J. Electrochem. Soc. 2015, 162, A2737; d) L. Madec, L. Ma, K. J. Nelson, R. Petibon, J.-P. Sun, I. G. Hill, J. R. Dahn, J. Electrochem. Soc. 2016, 163, A1001.
- [11] S. Klein, P. Bärmann, T. Beuse, K. Borzutzki, J. E. Frerichs, J. Kasnatscheew, M. Winter, T. Placke, *ChemSusChem* 2020, https://doi.org/10.1002/cssc.202002113.



\_\_\_\_ /FIATERIALS

ENERG

www.advancedsciencenews.com www.advenergymat.de

- [12] a) J.-P. Schmiegel, X. Qi, S. Klein, V. Winkler, M. Evertz, R. Nölle, J. Henschel, J. Reiter, L. Terborg, Q. Fan, C. Liang, S. Nowak, M. Winter, T. Placke, J. Electrochem. Soc. 2019, 166, A2910;
  b) Y. Dong, B. T. Young, Y. Zhang, T. Yoon, D. R. Heskett, Y. Hu, B. L. Lucht, ACS Appl. Mater. Interfaces 2017, 9, 20467.
- [13] a) C. Wang, L. Yu, W. Fan, J. Liu, L. Ouyang, L. Yang, M. Zhu, ACS Appl. Energy Mater. 2018, 1, 2647; b) Q. Lei, T. Yang, X. Zhao, W. Fan, W. Wang, L. Yu, S. Guo, X. Zuo, R. Zeng, J. Nan, J. Electroanal. Chem. 2019, 846, 113141; c) D. S. Hall, J. Li, K. Lin, N. Stakheiko, J. Baltazar, J. R. Dahn, J. Electrochem. Soc. 2019, 166, A793; d) D. S. Hall, T. Hynes, J. R. Dahn, J. Electrochem. Soc. 2018, 165, A2961.
- [14] R. Wang, X. Li, Z. Wang, H. Guo, T. Hou, G. Yan, B. Huang, J. Alloys Compd. 2015, 618, 349.
- [15] Y.-K. Choi, K.-i. Chung, W.-S. Kim, Y.-E. Sung, S.-M. Park, J. Power Sources 2002, 104, 132.
- [16] a) M. Winter, Z. Phys. Chem. 2009, 223, 1395; b) P. Verma, P. Maire,
   P. Novak, Electrochim. Acta 2010, 55, 6332.
- [17] a) G. Homann, L. Stolz, J. Nair, I. Cekic Laskovic, M. Winter, J. Kasnatscheew, Sci. Rep. 2020, 10, 4390; b) G. Homann, L. Stolz, M. Winter, J. Kasnatscheew, iScience 2020, 23, 101225.
- [18] a) L. Terborg, S. Weber, F. Blaske, S. Passerini, M. Winter, U. Karst, S. Nowak, J. Power Sources 2013, 242, 832; b) Y. P. Stenzel, F. Horsthemke, M. Winter, S. Nowak, Separations 2019, 6, 26.
- [19] P. Harte, M. Evertz, T. Schwieters, M. Diehl, M. Winter, S. Nowak, Anal. Bioanal. Chem. 2019, 411, 581.
- [20] a) B. S. Parimalam, A. D. MacIntosh, R. Kadam, B. L. Lucht, J. Phys. Chem. C 2017, 121, 22733; b) S. K. Heiskanen, J. Kim, B. L. Lucht, Joule 2019, 3, 2322.
- [21] Y. Bi, T. Wang, M. Liu, R. Du, W. Yang, Z. Liu, Z. Peng, Y. Liu, D. Wang, X. Sun, RSC Adv. 2016, 6, 19233.

- [22] Y. Li, B. Cheng, F. Jiao, K. Wu, ACS Appl. Mater. Interfaces 2020, 12, 16298.
- [23] K.-E. Kim, J. Y. Jang, I. Park, M.-H. Woo, M.-H. Jeong, W. C. Shin, M. Ue, N.-S. Choi, *Electrochem. Commun.* 2015, 61, 121.
- [24] W. Zhao, G. Zheng, M. Lin, W. Zhao, D. Li, X. Guan, Y. Ji, G. F. Ortiz, Y. Yang, J. Power Sources 2018, 380, 149.
- [25] a) P. Zou, Z. Lin, M. Fan, F. Wang, Y. Liu, X. Xiong, Appl. Surf. Sci. 2020, 504, 144506; b) P. Yan, J. Zheng, J. Liu, B. Wang, X. Cheng, Y. Zhang, X. Sun, C. Wang, J.-G. Zhang, Nat. Energy 2018, 3, 600
- [26] a) N. V. Faenza, Z. W. Lebens-Higgins, P. Mukherjee, S. Sallis, N. Pereira, F. Badway, A. Halajko, G. Ceder, F. Cosandey, L. F. J. Piper, G. G. Amatucci, *Langmuir* 2017, 33, 9333; b) Z. W. Lebens-Higgins, D. M. Halat, N. V. Faenza, M. J. Wahila, M. Mascheck, T. Wiell, S. K. Eriksson, P. Palmgren, J. Rodriguez, F. Badway, N. Pereira, G. G. Amatucci, T.-L. Lee, C. P. Grey, L. F. J. Piper, *Sci. Rep.* 2019, 9, 17720.
- [27] R. Nölle, K. Beltrop, F. Holtstiege, J. Kasnatscheew, T. Placke, M. Winter, Mater. Today 2020, 32, 131.
- [28] a) T. Schwieters, M. Evertz, M. Mense, M. Winter, S. Nowak, J. Power Sources 2017, 356, 47; b) T. Schwieters, M. Evertz, A. Fengler, M. Börner, T. Dagger, Y. Stenzel, P. Harte, M. Winter, S. Nowak, J. Power Sources 2018, 380, 194.
- [29] a) V. Kraft, M. Grützke, W. Weber, M. Winter, S. Nowak, J. Chromatogr. A 2014, 1354, 92; b) J. Henschel, F. Horsthemke, Y. P. Stenzel, M. Evertz, S. Girod, C. Lürenbaum, K. Kösters, S. Wiemers-Meyer, M. Winter, S. Nowak, J. Power Sources 2020, 447, 227370
- [30] B. Vortmann-Westhoven, M. Diehl, M. Winter, S. Nowak, Chromatographia 2018, 81, 995.